Comprehensive analysis of a palmitoylation-related prognostic signature in colorectal cancer: Implications for immune therapy and personalized treatment

XIAOKANG WANG[1*], JIAN LI[2*], ZI WANG[3] and QINGYUN WU[4]

[1]Department of Medical Oncology, Xianning Central Hospital, The First Affiliated Hospital of Hubei Institute of Science and Technology, Xianning, Hubei 437000, P.R. China; [2]Department of Gastroenterology, Xianning Central Hospital, The First Affiliated Hospital of Hubei Institute of Science and Technology, Xianning, Hubei 437000, P.R. China; [3]College of Medicine, Hubei Three Gorges Polytechnic, Yichang, Hubei 443000, P.R. China; [4]Department of Gastrointestinal Surgery, Xianning Central Hospital, The First Affiliated Hospital of Hubei Institute of Science and Technology, Xianning, Hubei 437000, P.R. China

Received December 11, 2024; Accepted March 26, 2025

DOI: 10.3892/ol.2025.15096

Abstract. Colorectal cancer (CRC) remains one of the leading causes of cancer-associated mortality worldwide. While immune checkpoint inhibitors have shown promise in treatment, there is a need for reliable biomarkers to predict patient prognosis and guide personalized therapies. Palmitoylation, a post-translational modification, has been implicated in various cancer processes, yet its role in CRC prognosis remains unclear. Transcriptome, survival, somatic mutation and copy number variation data were retrieved from The Cancer Genome Atlas, and the GSE17538 dataset was used for external validation. A palmitoylation-related risk signature was developed using univariate Cox regression, Least Absolute Shrinkage and Selection Operator and multivariate Cox regression analyses. Patients were stratified into high- and low-risk groups based on the median risk score. Prognostic accuracy was assessed using receiver operating characteristic curves and Kaplan-Meier overall survival (OS) analysis with validation in an independent cohort. Functional enrichment, immune cell infiltration and drug sensitivity analyses were performed to explore underlying mechanisms and therapeutic implications. Subsequently, keratin 8 pseudogene 12 (KRT8P12) overexpression was evaluated in HT29 cells, and knockdown HT29 cell lines were generated using lentivirus. Cell proliferation was assessed using Cell Counting Kit-8 and 5-ethynyl-2'-deoxyuridine assays, cell migration was evaluated by Transwell assay and cell apoptosis was assessed using Annexin-V/propidium iodide staining. A palmitoylation-related risk signature consisting of six genes (KRT8P12, ZDHHC3, PCOLCE2, MPP2, LARS2 and MMAA) was identified. High-risk patients exhibited significantly worse OS (HR=3.19; P<0.001) compared with low-risk patients. Immune cell infiltration analysis revealed enhanced immune activity in the low-risk group, which was associated with higher expression of immune checkpoint genes. Immunotherapy prediction models indicated that low-risk patients might benefit more from immune checkpoint inhibitors. Drug sensitivity analysis identified distinct drug response profiles between the high- and low-risk groups. Furthermore, *in vitro*, KRT8P12 promoted tumor cell proliferation and migration while inhibiting apoptosis. In conclusion, the present study confirmed the role of KRT8P12 as a palmitoylation-related gene in regulating CRC. In addition, the palmitoylation-associated risk signature may offer a promising tool for prognostic prediction in CRC and could guide personalized treatment strategies, including immune checkpoint inhibitors and targeted therapies.

Correspondence to: Professor Qingyun Wu, Department of Gastrointestinal Surgery, Xianning Central Hospital, The First Affiliated Hospital of Hubei Institute of Science and Technology, 228 Jingui Road, Xian'an, Xianning, Hubei 437000, P.R. China
E-mail: 13163415360@163.com

*Contributed equally

Abbreviations: CRC, colorectal cancer; TCGA, The Cancer Genome Atlas; CNV, copy number variation; LASSO, Least Absolute Shrinkage and Selection Operator; ROC, receiver operating characteristic; AUC, area under the curve; KM, Kaplan-Meier; OS, overall survival; TMB, tumor mutational burden; GO, Gene Ontology; KEGG, Kyoto Encyclopedia of Genes and Genomes; GISTIC, Genomic Identification of Significant Targets in Cancer; TIDE, Tumor Immune Dysfunction and Exclusion; GDSC, Genomics of Drug Sensitivity in Cancer; qPCR, quantitative PCR; FBS, fetal bovine serum; 2-BP, 2-bromopalmitate; CCK-8, Cell Counting Kit-8; PI, propidium iodide

Key words: CRC, palmitoylation, prognostic signature, immune cell infiltration, immunotherapy

Introduction

Colorectal cancer (CRC) is one of the most common and lethal malignancies worldwide (1). Despite advancements in early detection and treatment modalities, including surgery, chemotherapy and immunotherapy, the prognosis for patients

with advanced-stage CRC remains poor (2,3). Conventional prognostic factors, such as tumor stage and histopathological features, often fail to fully capture the complexity of the disease, underscoring the urgent need for novel biomarkers that can enhance risk stratification and inform therapeutic decisions (4,5). In previous years, the integration of molecular profiling and personalized treatment strategies has shown promise; however, patient responses to immune checkpoint inhibitors and targeted therapies remain highly variable (6), emphasizing the necessity for biomarkers that predict therapeutic efficacy.

Palmitoylation, a dynamic post-translational modification involving the reversible attachment of fatty acid chains to cysteine residues of proteins, serves a critical role in regulating protein function, membrane localization and cellular signaling (7,8). This modification is essential for several cellular processes, including signal transduction, protein trafficking and cellular adhesion. Emerging evidence has suggested that altered palmitoylation contributes to the pathogenesis of several types of cancer, including CRC, by modulating key oncogenic signaling pathways, enhancing cell survival and promoting immune evasion (9,10). Palmitoylation of ERb can activate 17β-estradiol, thereby activating the p38/MAPK pathway to promote apoptosis of human colon adenocarcinoma DLD-1 cells (11). However, it has also been observed that the palmitoylation of ERb or inhibition of p38/MAPK signaling promotes the proliferation of CRC cells (12). Therefore, palmitoylation serves a notable biological role in CRC. In addition, several studies have demonstrated that Wnt2B palmitoylation alters its cellular localization, indirectly affecting Wnt signaling (13), and the level of Wnt2B palmitoylation in mitochondria is negatively associated with the occurrence of intestinal tumors (14). The palmitoylation of YES in the SH4 domain regulates its localization in the cholesterol-rich membrane microstructure domain, which enhances the phosphorylation of upstream regulatory factors EGFR, SHC and SHP2 in Ras/MAPK signaling, thereby inhibiting colon cancer cell adhesion and promoting invasion (15). Therefore, palmitoylation can regulate the activation of p38/MAPK, Wnt and Ras/MAPK signaling pathways to control the proliferation and metastasis of CRC.

The ZDHHC family, a key enzyme involved in regulating palmitoylation, also serves a notable role in the progression of CRC. ZDHHC20 is one of the key ZDHHC enzymes located on the plasma membrane. Draper and Smith (16) demonstrated that the mRNA levels of ZDHHC20 in ovarian cancer, breast cancer, colon cancer, kidney cancer and prostate cancer were markedly higher compared with those in organ-matched normal tissues. In addition, Fas (also known as CD95) is palmitoylated by ZDHHC7 at Cys199 to increase its stability and lipid raft localization; notably, inhibition of Fas palmitoylation by small interfering RNA knockout of ZDHHC7 can promote CRC cell lines to escape FasL-induced cell death (17). However, the precise role of palmitoylation in CRC progression and its potential as a prognostic marker have yet to be comprehensively explored. With the advent of bioinformatics approaches, the integration of multi-omics data has facilitated the identification of molecular signatures that can predict clinical outcomes and therapeutic responses, offering novel options for personalized medicine (18).

The present study aimed to establish a palmitoylation-related prognostic signature for CRC by performing a systematic analysis of transcriptomics, clinical and genomics data. Our findings offer valuable insights into the role of palmitoylation-related genes in CRC and identify potential biomarkers for prognosis and immunotherapy strategies.

Materials and methods

Data acquisition. Transcriptome data, survival information, somatic mutation data and copy number variation (CNV) data for patients with CRC were retrieved from The Cancer Genome Atlas (TCGA) database (https://portal.gdc.cancer.gov/). After excluding patients with a survival time of <30 days, a total of 418 patients were included in the subsequent analyses, and 41 healthy individuals served as negative controls. The GSE17538 dataset, used as an external validation cohort, was obtained from the Gene Expression Omnibus database (https://www.ncbi.nlm.nih.gov/geo/). Additionally, a list of 3,532 palmitoylation-related genes was extracted from the GeneCards database (https://www.genecards.org/).

Identification of a palmitoylation-related risk signature. To identify prognostic genes, univariate Cox regression analysis was first performed, with a significance threshold of $P<0.001$. To enhance the selection process, Least Absolute Shrinkage and Selection Operator (LASSO) regression was performed using the glmnet package (https://cran.r-project.org/web/packages/glmnet/index.html) in R studio 4.3.1 version software (https://cran.rstudio.com/). LASSO regression analysis was performed employing 10-fold cross-validation to determine the optimal regularization parameter (λ). The λ value selected was the one that maximized model fit while simultaneously minimizing the risk of overfitting. Samples with missing or insufficient clinical data were excluded during univariate Cox analysis, ensuring the accuracy of LASSO regression analysis, which was applied to select the most relevant prognostic genes from the initial set of identified candidates. Following this, a multivariate Cox regression analysis was performed to establish a palmitoylation-related prognostic model. In addition, the differences in the expression profiles of the six model genes between normal and CRC tissues were assessed and were depicted in a heatmap, which was generated using the pheatmap package (https://cran.r-project.org/web/packages/pheatmap/index.html) in R studio 4.3.1 version software (19). Patients in both the training and validation cohorts were stratified into high- and low-risk groups based on the median risk score derived from the model. The receiver operating characteristic (ROC) curve was generated to evaluate the prognostic performance of the model, with the area under the curve (AUC) used to assess sensitivity and specificity. Kaplan-Meier (KM) OS analysis was subsequently performed to assess the association between the palmitoylation-related risk signature and OS. The OS of patients was evaluated by KM analysis using the survival package (https://cran.r-project.org/web/packages/survival/index.html) of R studio 4.3.1 version software (19); log-rank test was used to obtain P-values. Finally, the prognostic impact of the expression levels of individual model genes was evaluated to understand their contribution to patient survival outcomes.

Assessment of the prognostic model. Firstly, the expression levels of the model genes were compared between CRC tissues and adjacent normal tissues to identify potential alterations associated with CRC. Subsequently, the correlation between the expression levels of each model gene and the risk score was assessed to understand their contributions to the risk stratification and their prognostic relevance in patients with CRC with Pearson correlation analysis. A nomogram was constructed using the 'rms' package (https://cran.r-project.org/web/packages/rms/index.html) in R studio 4.3.1 version software incorporating clinical features, such as tumor (T) stage, lymph node (N) stage, clinical stage, age, sex and risk score, to predict individualized prognosis. Differences in clinical characteristics, including survival status and tumor stage [T, N and metastasis (M) stages], were then compared between the high- and low-risk groups to evaluate their potential impact on prognosis. Finally, the prognostic accuracy of the model was validated using the independent GSE17538 validation dataset, and survival outcomes for patients in the high- and low-risk groups were compared to assess the robustness of the risk signature.

Functional enrichment and TMB analyses. To explore the molecular mechanisms underlying the palmitoylation-related risk signature, Gene Ontology (GO) and Kyoto Encyclopedia of Genes and Genomes (KEGG) pathway enrichment analyses were performed using the ClusterProfiler package (https://www.bioconductor.org/packages/release/bioc/html/clusterProfiler.html) (20). These analyses aimed to identify key biological processes and signaling pathways associated with the signature. Somatic mutation data for patients with CRC were converted to Mutation Annotation Format using the maftools R package for the subsequent TMB analysis (21). Mutational landscapes were subsequently compared between the high- and low-risk groups to assess potential differences in mutation profiles. Additionally, the TMB was calculated for each sample, and the difference in prognosis between the high-TMB and low-TMB groups was examined to investigate the potential impact of TMB on the prognostic model (22).

Identification of genomic alterations through CNV analysis. CNV was assessed using the Genomic Identification of Significant Targets in Cancer (GISTIC) algorithm (23). This tool identifies genomic regions with recurrent amplifications or deletions across a set of samples, assigning statistical significance to these alterations. The GISTIC analysis aimed to uncover potential oncogenes or tumor suppressor genes associated with CRC. The results of the CNV analysis were visualized through copy number plots, highlighting the genomic regions with significant gains or losses and their potential relevance to cancer development.

Immune cell infiltration analysis. Immune cell infiltration and immune function scores were assessed using the single-sample Gene Set Enrichment Analysis algorithm (24), which calculates rank scores for each gene based on gene expression profiles. Differences in immune cell infiltration and immune function scores between the high- and low-risk groups were then compared. A comparative analysis of the differential expression of 50 immune checkpoint genes between the two groups was also performed using the CIBERSORT algorithm (https://github.com/Moonerss/CIBERSORT) (25).

Immunotherapy and drug sensitivity analysis. Due to the critical role of immune checkpoint inhibitors in CRC treatment, the correlation between the risk score and the expression levels of programmed cell death protein 1 (PD-1), programmed death-ligand 1 (PD-L1), cytotoxic T-lymphocyte associated protein 4 (CTLA4) and T cell immunoreceptor with Ig and ITIM domains (TIGIT) was examined. The Tumor Immune Dysfunction and Exclusion (TIDE) algorithm (26) was used to predict the response of high- and low-risk groups to immune checkpoint inhibitors. TIDE analyzed gene expression data to assess tumor immune evasion mechanisms, calculate immune evasion scores and predict the likelihood of response to immune therapy for each group (27). Subsequently, SubMap analysis (http://cloud.genepattern.org/gp) was performed to further evaluate the immune therapy responsiveness in the high- and low-risk groups, identifying potential differences in treatment outcomes (28). Finally, drug sensitivity was assessed using the pRRophetic package (29), which calculated the half-maximal inhibitory concentration values for various agents from the Genomics of Drug Sensitivity in Cancer (GDSC) database (http://www.cancerrxgene.org), comparing sensitivity between the high- and low-risk patient groups.

Cell culture and transduction. HCT116 (cat. no. CCL-247) and HT29 (cat. no. HTB-38) cell lines were purchased from American Type Culture Collection. Cells were cultured in 90% Dulbecco's Modified Eagle Medium (DMEM; Gibco; Thermo Fisher Scientific, Inc.) supplemented with 10% fetal bovine serum (FBS; Gibco; Thermo Fisher Scientific, Inc.) and 1% penicillin/streptomycin (Shanghai Yeasen Biotechnology Co., Ltd.), and were maintained in a humidified incubator at 37˚C with 5% CO_2. Cells were passaged twice, resulting in the use of third-generation cells for subsequent experiments. A lentivirus-based short hairpin RNA (shRNA) approach was employed using three distinct shRNA sequences. These shRNA sequences were cloned into the pLKO.1 lentiviral vector with the aim of downregulating the expression of KRT8P12 in HCT116 cells. In addition, full-length KRT8P12 cDNA was synthesized and cloned into the pLV-CMV-MCS-PGK-Puro lentiviral overexpression vector for the purpose of inducing KRT8P12 overexpression in HT29 cells. Both pLKO.1 and pLV-CMV-MCS-PGK-Puro vectors were procured from Beijing Zhongyuan, Ltd. Lentiviral particles were produced by co-transfecting 293T cells with a packaging plasmid mix (REV:VSVG:PMDL, 2:3:5) in 400 μl serum-free DMEM, 1.5 μg core plasmid and 1.5 μg viral packaging plasmid with 6 μl TurboFect (TurboFect:plasmid, 2:1; cat. no. R0532; Fermentas; Thermo Fisher Scientific, Inc.) at 37˚C. The reagent was mixed thoroughly and let sit for 20 min before being added to the cells. Then the cells were harvested 48 h post-transfection. The resultant virus-containing supernatant was collected and filtered. This supernatant was subsequently utilized to infect HCT116 and HT29 cells. Briefly, the HCT116 and HT29 cells were seeded into 6-well plates and cultured until they reached 60-70% confluence, after which, lentiviral particles (multiplicity of infection=10) along with poly-L-lysine (8 μg/ml) were added to enhance viral transduction efficacy. The cells were co-cultured with the virus for 12 h at 37˚C, after which they were replaced with fresh culture medium. A total of 48 h post-infection, stable transductants were selected; puromycin

was the antibiotic used to confirm successful transduction. The original concentration of puromycin used was 1 mg/ml and 2 μg/ml puromycin was used for selection and maintenance. All culture processes were conducted under conditions of 37˚C and 5% CO_2. The sequences for KRT8P12 knockdown and overexpression are shown in Table SI. HCT116, HT29, sh-KRT8P12 and OE-KRT8P12 cells were cultured in DMEM, supplemented with 10% FBS and 1% penicillin-streptomycin. Cells without any treatment served as a blank control group, whereas a pLKO.1 vector containing a nontargeting shRNA and an empty pLV-CMV-MCS-PGK-Puro vector served as negative controls for knockdown and overexpression, respectively. Cells were maintained at 37˚C in a 5% CO_2 incubator, with medium changes every 2-3 days. For passaging, cells were detached using 0.25% trypsin-EDTA, centrifuged at 80 x g for 3 min at room temperature and reseeded at a 1:3 to 1:6 dilution. When freezing, cells were suspended in a cryoprotectant medium (10% DMSO, 20% FBS and 70% DMEM) and stored at -80˚C or in liquid nitrogen for long-term preservation.

RNA extraction and reverse transcription-quantitative PCR (RT-qPCR). Total RNA was isolated from cell samples utilizing TRIzol® reagent (Invitrogen; Thermo Fisher Scientific, Inc.), and was subsequently converted into cDNA employing a cDNA synthesis kit (Vazyme Biotech Co., Ltd.) according to the manufacturer's protocol. qPCR was conducted using SYBR Green qRT-PCR Master Mix (Vazyme Biotech Co., Ltd.), with GAPDH serving as the internal control for normalization. qPCR was performed as follows: Pre-denaturation for 2 min at 95˚C, followed by 40 cycles of denaturation for 20 sec at 94˚C, annealing for 20 sec at 60˚C and extension for 20 sec at 72˚C. The $2^{-\Delta\Delta Cq}$ method was used for quantification (30). The primer sequences used are listed in Table SII.

Cell Counting Kit-8 (CCK-8) cell proliferation assay. To assess cell proliferation, the CCK-8 assay (Beijing Solarbio Science & Technology Co., Ltd.) was performed according to the manufacturer's instructions. CRC cells were seeded in 96-well plates at a density of $1x10^4$ cells/well and allowed to adhere overnight. 2-Bromopalmitate (2-BP) is a broad-spectrum inhibitor of protein palmitoylation and was purchased from MilliporeSigma. Before CCK-8 assay, the cells underwent different experimental conditions (sh-KRT8P12 or OE-KRT8P12 transduction, and 2-BP treatment). For 2-BP treatment, cells were treated with 50 μM 2-BP for 1 h at 37˚C to inhibit palmitoylation in CRC cells. After 24, 48 or 72 h incubation, 10 μl CCK-8 solution was added to each well and the cells were incubated for an additional 2 h at 37˚C. The absorbance was measured at 450 nm using a microplate reader. The relative cell proliferation was calculated by comparing the absorbance values of treated cells to the control group. Each experiment was performed in triplicate and repeated at least three times.

5-Ethynyl-2'-deoxyuridine (EdU) cell proliferation assay. To evaluate cell proliferation, the EdU incorporation assay (cat.no.E-CK-A376; Elabscience; Elabscience Bionovation Inc.) was performed. CRC cells were seeded in 24-well plates at a density of $2x10^4$ cells/well and allowed to adhere overnight. After treatment under different experimental conditions (sh-KRT8P12 or OE-KRT8P12 transduction, and 2-BP treatment), the cells were incubated with 10 μM EdU for 2 h at 37˚C in a 5% CO_2 incubator. Following incubation, cells were fixed with 4% paraformaldehyde for 15 min at room temperature, and were then permeabilized with 0.3% Triton X-100 and stained with Click-iT EdU reaction cocktail, according to the manufacturer's protocol. The cell nuclei were counterstained with Hoechst to visualize the total cells. Proliferating cells were observed by fluorescence microscopy. Each experiment was performed in triplicate and repeated at least three times.

Transwell cell migration assay. To assess cell migration, a Transwell assay was performed using 24-well plates with a polycarbonate membrane insert (pore size, 8 μm). CRC cells were seeded into the upper chamber of the Transwell insert at a density of $1x10^4$ cells/well in 200 μl serum-free medium. The lower chamber was filled with 600 μl complete medium containing 10% FBS to act as a chemoattractant. After incubating for 24 h at 37˚C in a 5% CO_2 incubator, non-migrated cells on the upper surface of the membrane were gently removed using a cotton swab. Migrated cells on the lower surface of the membrane were fixed with 4% paraformaldehyde for 10 min and stained with 0.1% crystal violet solution for 15 min at room temperature. Images of the stained cells were then captured using an inverted light microscope, and the number of migrated cells was quantified by counting the cells in five random fields per well. Each experiment was performed in triplicate and repeated at least three times.

Flow cytometric analysis of apoptosis. To assess apoptosis, flow cytometric analysis was performed using an Annexin V-FITC/PI apoptosis detection kit (cat. no. C1062S; Beyotime Institute of Biotechnology). CRC cells were seeded in 6-well plates at a density of $1x10^5$ cells/well and underwent different experimental conditions: sh-KRT8P12 or OE-KRT8P12 transduction, and 2-BP treatment (50 μM 2-BP for 1 h at 37˚C in a 5% CO_2 incubator). After treatment, the cells were harvested by trypsinization, washed twice with phosphate-buffered saline and resuspended in 1X binding buffer at a concentration of $1x10^6$ cells/ml. Subsequently, 5 μl Annexin V-FITC and 5 μl PI were added to a 100-μl cell suspension, and the mixture was incubated in the dark at room temperature for 15-20 min. After incubation, 400 μl 1X binding buffer was added to each sample. The stained cells were analyzed using a FACSCalibur flow cytometer (BD Biosciences). Annexin V-positive and PI-negative cells were considered early apoptotic, whereas Annexin V-positive and PI-positive cells were considered late apoptotic or necrotic. The percentage of apoptotic cells was calculated by summing the early and late apoptotic population using FlowJo version 10.8.1 (BD Biosciences). Each experiment was performed in triplicate and repeated at least three times.

Statistical analysis. All the bioinformatics analyses in this manuscript were conducted using R studio 4.3.1 version software. Data were analyzed using GraphPad Prism 9.0 software (Dotmatics). All experiments were performed in triplicate and results are presented as the mean ± standard deviation. Differences between two groups were analyzed by unpaired Student's t-test. Differences between more than two groups were analyzed using one-way ANOVA with the Bonferroni post hoc test. $P<0.05$ was considered to indicate a statistically

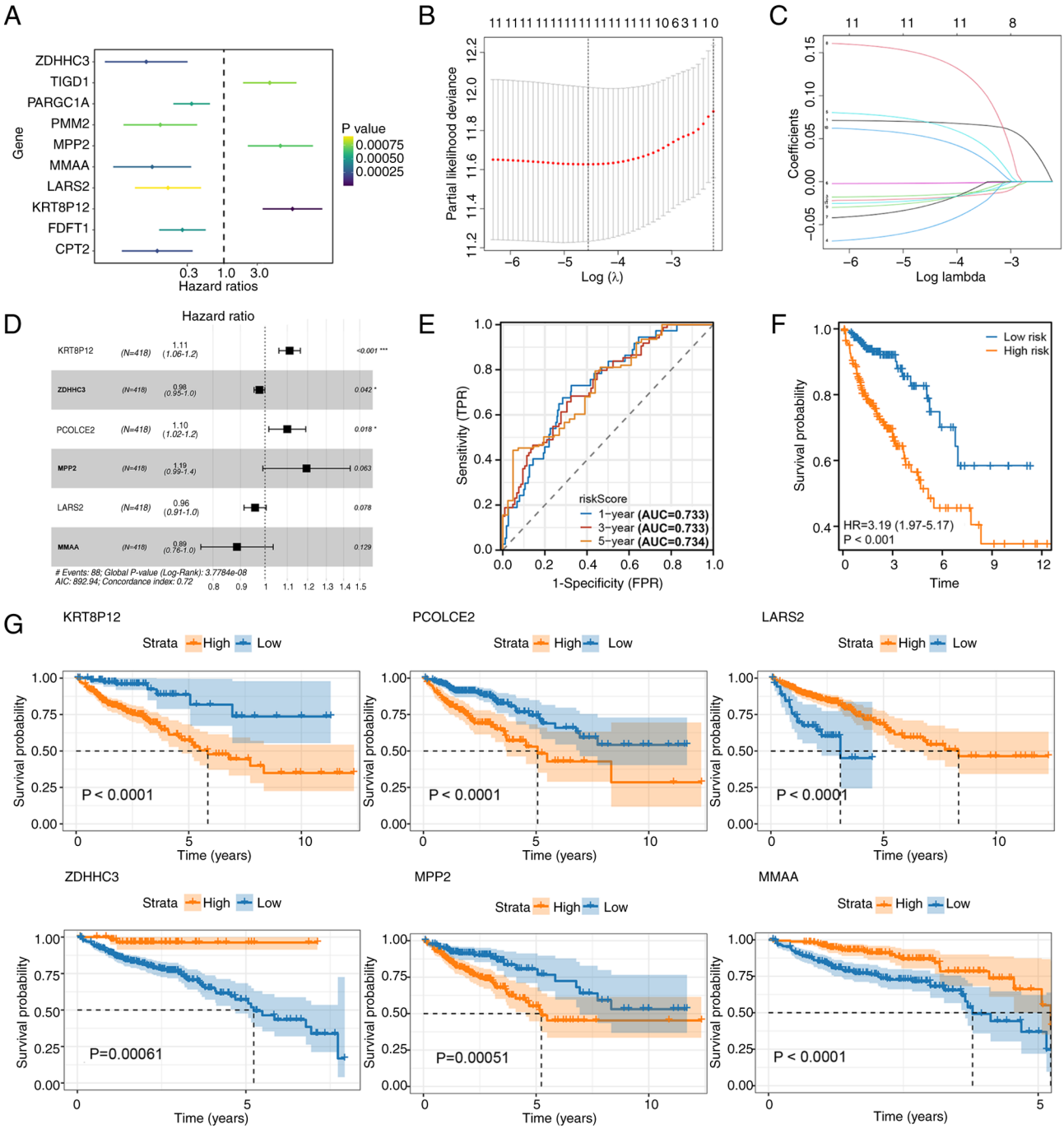

Figure 1. Identification of a palmitoylation-related risk signature. (A) Univariate Cox regression analysis of palmitoylation-related genes identified 10 prognostic candidates (P<0.001). ZDHHC3, PARGC1A, PMM2, MMAA, LARS2, FDFT1 and CPT2 were protective factors (HR <1), while TIGD1, MPP2 and KRT8P12 were risk factors (HR >1). (B) LASSO analysis for dimensionality reduction. (C) LASSO analysis for selecting key prognostic genes. (D) Multivariate Cox regression modeling incorporating six genes (KRT8P12, ZDHHC3, PCOLCE2, MPP2, LARS2 and MMAA) to construct the risk signature. (E) Time-dependent receiver operating characteristic curves for 1-, 3- and 5-year survival predictions, with AUC values of 0.733, 0.733 and 0.734, respectively. (F) KM survival analysis of high- and low-risk groups based on the risk score, showing significantly worse survival in the high-risk group (HR=3.19; P<0.001). (G) KM survival curves of the six model genes (KRT8P12, ZDHHC3, PCOLCE2, MPP2, LARS2 and MMAA), each demonstrating significant prognostic value. *P<0.05; ***P<0.001. LASSO, Least Absolute Shrinkage and Selection Operator; KM, Kaplan-Meier; AUC, area under the curve; KRT8P12, keratin 8 pseudogene 12.

significant difference. All experiments were repeated at least three times to ensure reproducibility.

Results

Identification of a palmitoylation-related risk signature. Univariate Cox regression analysis identified 10 palmitoylation-related genes significantly associated with OS (Fig. 1A). Among these, ZDHHC3, PARGC1A, PMM2, MMAA, LARS2, FDFT1 and CPT2 were protective factors (HR <1), while TIGD1, MPP2 and KRT8P12 were risk factors (HR >1). To refine the model, LASSO regression analysis was performed, narrowing the candidate genes to a manageable subset for multivariate analysis (Fig. 1B). Multivariate

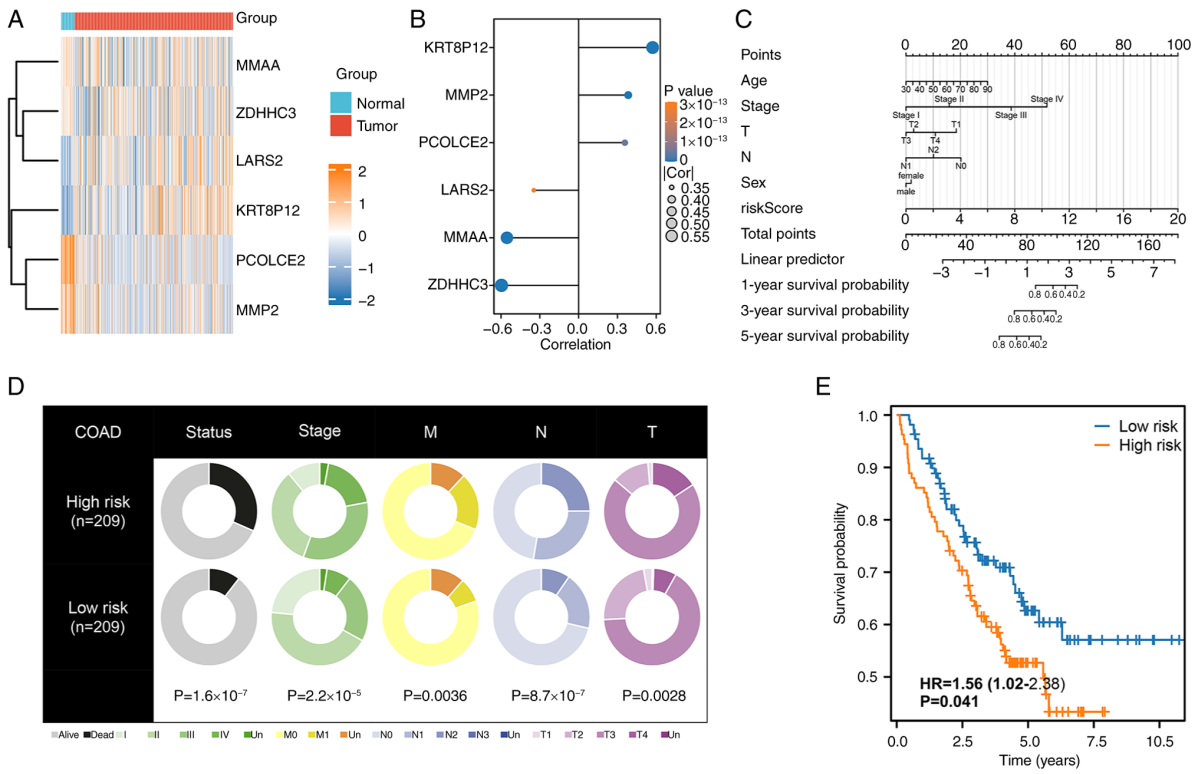

Figure 2. Validation and clinical implications of the palmitoylation-related risk signature. (A) Heatmap depicting the differential expression of the six model genes between normal and colorectal cancer samples, illustrating significant alterations. (B) Lollipop plot showing the correlation between model gene expression and the risk score, with KRT8P12 exhibiting the strongest positive correlation. (C) Nomogram integrating clinical parameters, including age, stage, T stage, N stage, sex and risk score, to provide a comprehensive prognostic tool. (D) Comparative analysis of clinical features between high- and low-risk groups, demonstrating worse prognoses and more advanced clinical stages (stage, T, N and M stages) in the high-risk group. (E) Kaplan-Meier survival analysis validating the risk model in the GSE17538 dataset, showing significantly poorer survival outcomes for the high-risk group (P<0.05). KRT8P12, keratin 8 pseudogene 12; T, tumor; N, lymph node; M, metastasis; COAD, colon adenocarcinoma.

Cox regression modeling ultimately identified six critical genes, KRT8P12, ZDHHC3, PCOLCE2, MPP2, LARS2 and MMAA, to construct a palmitoylation-related risk signature (Fig. 1C and D). The risk score formula was defined as follows: RiskScore=(KRT8P12 x 0.105257166581237)-(ZDHHC3 x 0.0240068245440265)+(PCOLCE2 x 0.0952477383419697)+(MPP2x0.177664830643707)-(LARS2x0.0426016477398653)-(MMAA x 0.1200626992622).

The prognostic efficacy of the model was evaluated using time-dependent ROC curves, which yielded AUC values of 0.733, 0.733 and 0.734 for 1-, 3- and 5-year survival, respectively (Fig. 1E). KM OS analysis demonstrated that patients in the high-risk group exhibited significantly worse survival compared with those in the low-risk group (Fig. 1F). Furthermore, individual KM analyses of the six model genes confirmed their prognostic relevance, with all genes significantly associated with survival outcomes (Fig. 1G). These findings indicated the robust prognostic utility of the palmitoylation-related risk signature in stratifying patients with CRC.

Validation and clinical relevance of the palmitoylation-related risk signature. The heatmap of six model genes, highlighted their potential roles in tumor biology (Fig. 2A). Correlation analysis revealed a strong positive association between KRT8P12 expression and the risk score, making it the most influential contributor to the risk signature, as shown in the lollipop plot (Fig. 2B). To facilitate individualized prognostic prediction, a nomogram integrating key clinical parameters, i.e. age, stage, T stage, N stage, sex and the risk score, was constructed, providing a visual tool for risk stratification (Fig. 2C). Analysis of clinical characteristics between high- and low-risk groups demonstrated that patients in the high-risk group had significantly worse prognoses and were more likely to present with advanced disease, including higher stage, T stage, N stage and M stage classifications (Fig. 2D). The prognostic utility of the model was further validated in the independent GSE17538 dataset, where Kaplan-Meier OS analysis confirmed that patients in the high-risk group experienced significantly worse outcomes (Fig. 2E). These findings underscore the robustness of the palmitoylation-related risk signature and its strong association with disease progression and survival outcomes.

Functional enrichment and mutation landscape analyses between risk groups. GO and KEGG analyses revealed both common and unique pathways in the high- and low-risk groups. Shared pathways between the groups included 'olfactory transduction' and 'olfactory receptor activity', underscoring certain overlapping molecular mechanisms (Fig. 3A and B). However, distinct pathways were observed in each group: The high-risk group was significantly enriched for 'intermediate filament' and 'sensory perception of smell', whereas the low-risk group exhibited unique enrichment in 'odorant binding' and 'detection of chemical stimulus involved in sensory perception'.

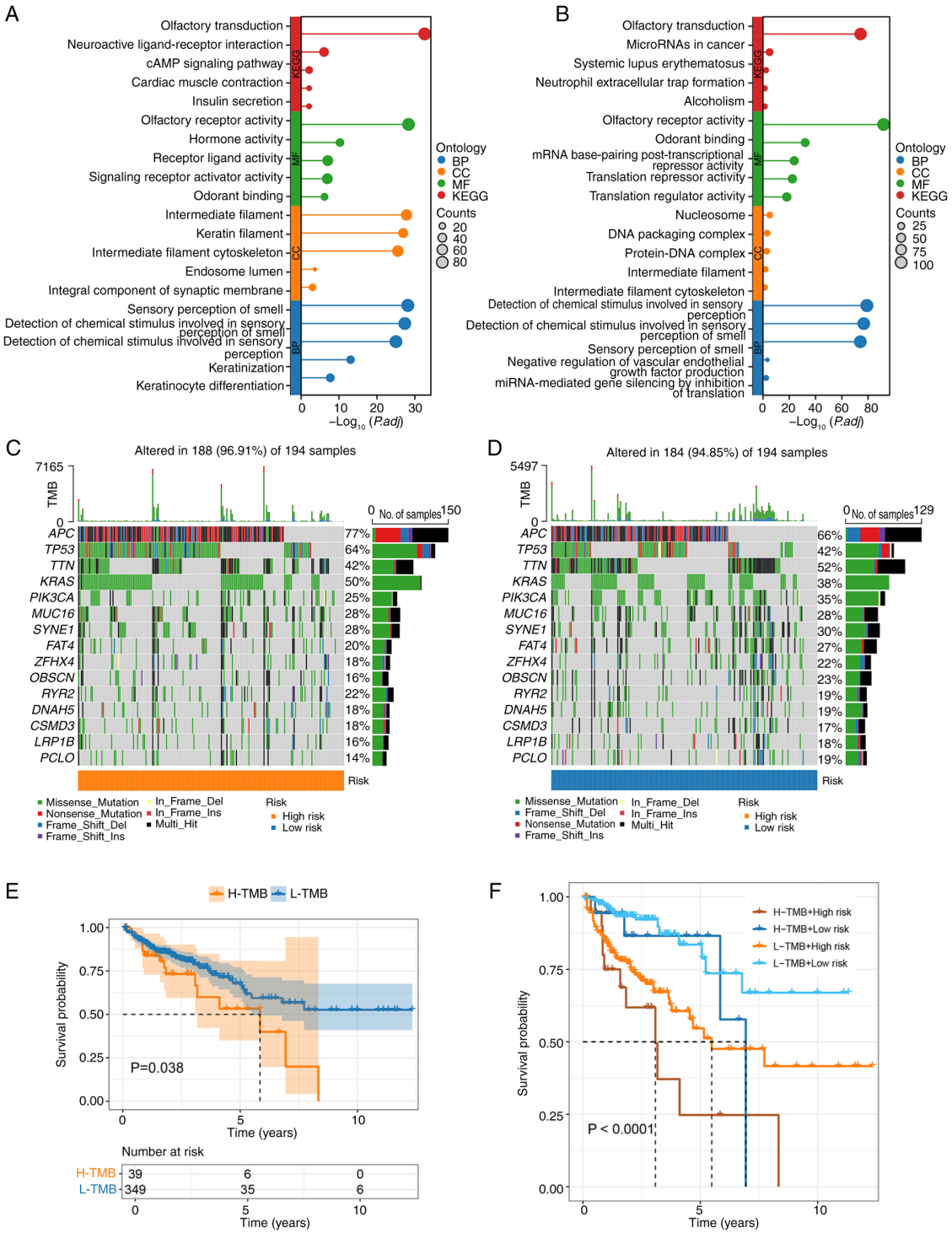

Figure 3. Functional enrichment and mutational landscape analysis between risk groups. (A) GO and KEGG enrichment analyses of the high-risk group showing significant enrichment in pathways such as 'olfactory transduction', 'olfactory receptor activity', 'intermediate filament' and 'sensory perception of smell'. (B) GO and KEGG enrichment analyses of the low-risk group highlighting overlapping pathways ('olfactory transduction' and 'olfactory receptor activity') as well as unique pathways, including 'odorant binding' and 'detection of chemical stimulus involved in sensory perception'. (C) Waterfall plot illustrating the mutation profile of the high-risk group, with the top five most frequently mutated genes being APC, TP53, TTN, KRAS and PIK3CA. (D) Waterfall plot of the mutation profile in the low-risk group, showing similar mutation frequencies to the high-risk group. (E) KM survival curve comparing patients with high-TMB and low-TMB, indicating significantly worse survival in the high-TMB group (P=0.038). (F) KM survival curve combining TMB status and risk group stratification, revealing the worst survival outcomes in the high-risk/high-TMB subgroup (P<0.0001). KM, Kaplan-Meier; GO, Gene Ontology; KEGG, Kyoto Encyclopedia of Genes and Genomes; TMB, tumor mutational burden; BP, biological process; CC, cellular component; MF, molecular function.

These findings suggested distinct biological underpinnings contributing to the differential prognosis between the two groups. Somatic mutation landscape analyses demonstrated no significant differences in mutation frequencies between the high- and low-risk groups, with the five most frequently mutated genes being APC, TP53, TTN, KRAS and PIK3CA in both groups (Fig. 3C and D). KM OS analysis stratified by TMB revealed that patients with high TMB had significantly

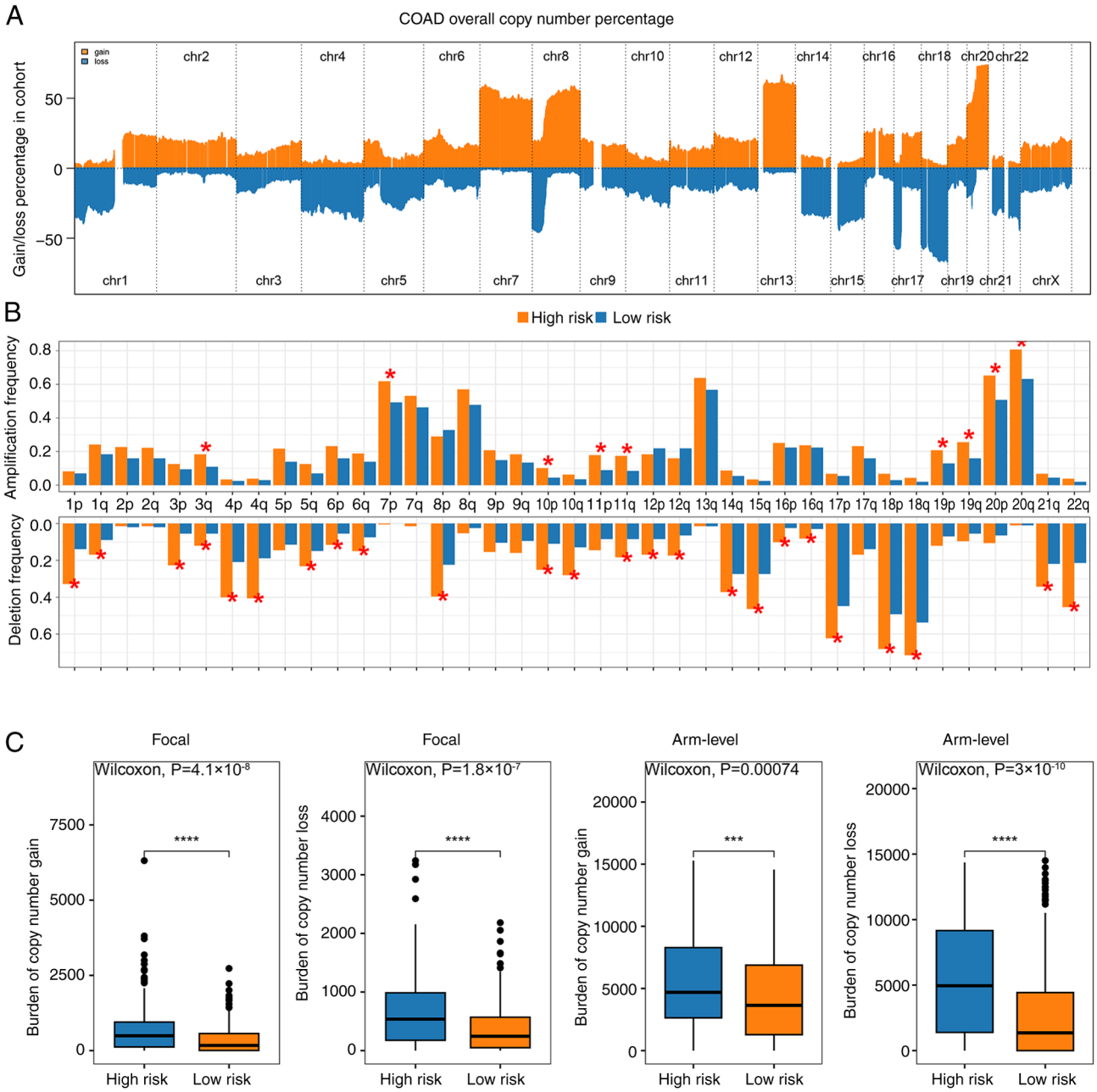

Figure 4. CNV analysis in high- and low-risk groups. (A) Percentages of copy number gains and losses in high- and low-risk groups, demonstrating significant differences in distribution. (B) Frequency of amplification and deletion events, showing a higher frequency in the high-risk group compared with in the low-risk group. (C) Burden of copy number gains and losses at focal and arm levels, with the high-risk group exhibiting significantly elevated CNV burden across both levels. *P<0.05; ***P<0.001; ****P<0.0001. CNV, copy number variation; COAD, colon adenocarcinoma.

worse survival outcomes compared with those with low TMB (Fig. 3E). Furthermore, combining TMB status with risk score stratification provided a more refined prognostic insight: Patients with high-risk/high-TMB demonstrated the worst survival outcomes, highlighting a strong interplay between mutational burden and risk group in determining prognosis (Fig. 3F). These results emphasized the clinical relevance of integrating genetic and molecular signatures for precise prognostic prediction in patients with CRC.

CNV analysis in high- and low-risk groups. CNV analysis uncovered distinct genomic alterations between high- and low-risk groups. The percentages of copy number gains and losses displayed significant differences, with the high-risk group showing a notably different distribution compared with the low-risk group (Fig. 4A). Additionally, the high-risk group exhibited a higher frequency of amplification and deletion events, reflecting greater genomic instability (Fig. 4B). Further analysis of CNV burden at both focal and arm levels revealed that the high-risk group consistently demonstrated significantly elevated levels of copy number gains and losses compared with the low-risk group (Fig. 4C). These findings suggested that the increased CNV burden in the high-risk group may contribute to the worse prognosis observed in these patients, highlighting the potential role of genomic instability in risk stratification.

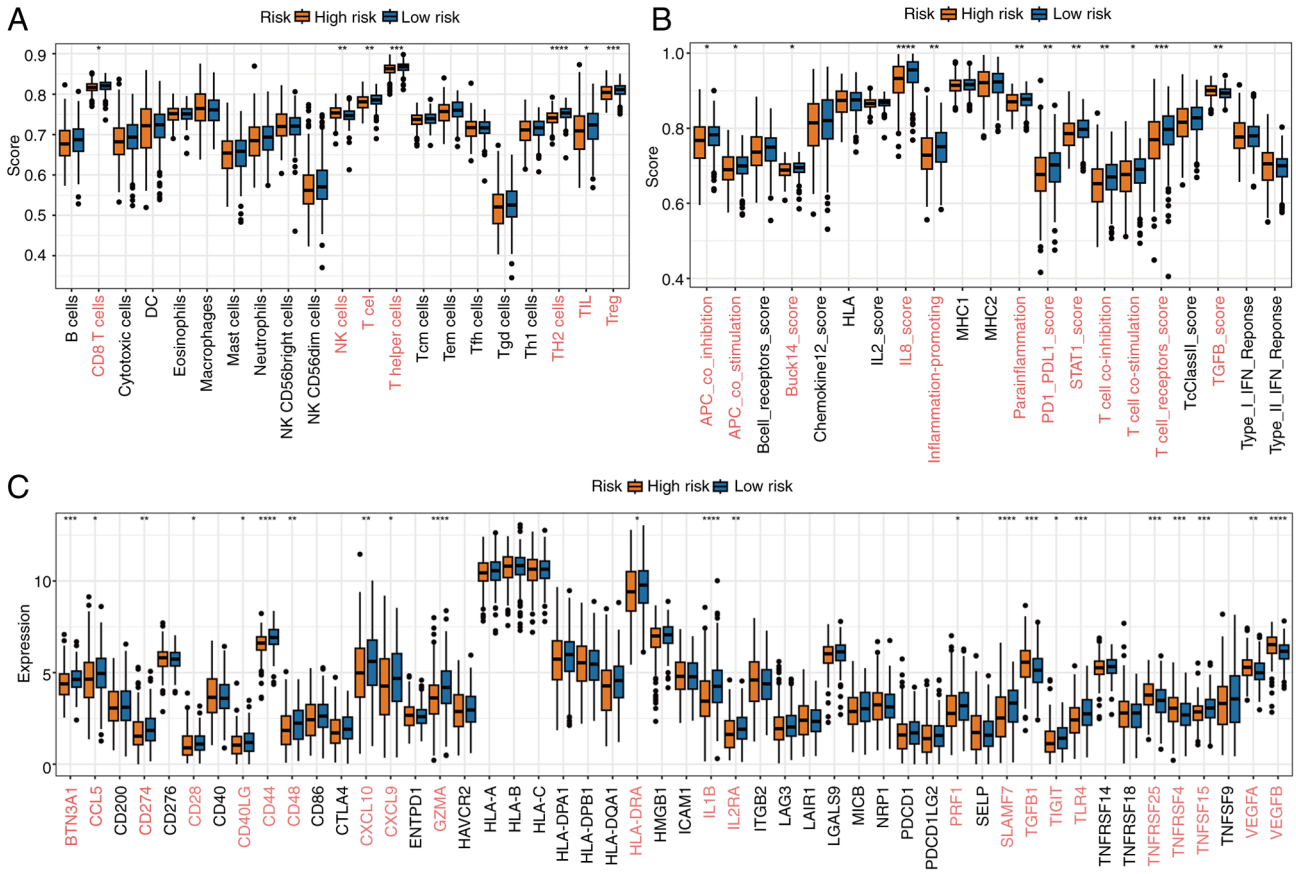

Figure 5. Immune cell infiltration analysis in high- and low-risk groups. (A) Differential analysis of immune cell abundance between high- and low-risk groups, revealing significantly higher levels of immune cell infiltration in the low-risk group. (B) Comparative analysis of immune functional pathways, showing higher activity of immune-related functions in the low-risk group. (C) Differential expression analysis of common immune checkpoint genes, indicating an overall trend of higher expression in the low-risk group. Significant differences are highlighted in red. *P<0.05; **P<0.01; ***P<0.001; ****P<0.0001.

Infiltration and treatment prediction analysis. Immune cell infiltration analysis demonstrated notable differences in immune cell abundance between the high- and low-risk groups. Differential expression analysis revealed that most immune cell types were significantly more abundant in the low-risk group, suggesting enhanced immune activity (Fig. 5A). Similarly, functional pathway analysis indicated that key immune-related processes were more active in the low-risk group, further highlighting the distinct immune landscape between the two groups (Fig. 5B). Additionally, the expression levels of common immune checkpoint genes exhibited significant differences between the groups, with an overall trend of higher expression in the low-risk group, reflecting its more robust immune environment (Fig. 5C).

Treatment prediction analysis further elucidated the clinical implications of the risk signature. Correlation analysis of the risk score with the expression of immune checkpoint genes, including PD-1, CD274 (PD-L1), CTLA4 and TIGIT, revealed a strong negative association, with higher expression of these genes in the low-risk group; however, although the association was observed, it was not statistically significant (Fig. 6A). TIDE analysis supported these findings, showing that low-risk patients had lower TIDE scores, indicating a greater likelihood of responding to immune checkpoint inhibitors (Fig. 6B). SubMap analysis further demonstrated that low-risk patients might benefit more from immunotherapy (Fig. 6C).

In addition to immunotherapy, drug sensitivity analysis based on the GDSC database identified significant differences in response to several therapeutic agents. The analysis highlighted the top eight drugs with the most pronounced differences in sensitivity between the high- and low-risk groups, with the drug sensitivity being lower in the low risk group, underscoring distinct drug response profiles associated with the risk score (Fig. 6D). Vinblastine is a microtubule inhibitor that prevents cell mitosis by inhibiting microtubule polymerization, which is primarily used for treating Hodgkin's lymphoma, non-Hodgkin's lymphoma and certain solid tumors (31). Afatinib is an irreversible tyrosine kinase inhibitor that targets EGFR mutations, mainly used in non-small cell lung cancer (32). 5-Fluorouracil is a pyrimidine analog that inhibits thymidylate synthase, thus disrupting DNA synthesis, which is widely used in CRC, gastric and breast cancer (33). Gemcitabine is a nucleoside analog that inhibits DNA replication, commonly used in pancreatic, lung and breast cancer (34). YK-4-279 is an EWS-FLI1 inhibitor, primarily targeting EWS-FLI1 fusion gene-associated tumors such as Ewing sarcoma (35). Vincristine is a microtubule inhibitor that blocks mitosis, and is mainly used for leukemia, lymphoma and certain solid tumors (36). Vinorelbine, a vinca alkaloid, inhibits microtubule function and is mainly used for non-small cell lung cancer and breast cancer (37). GSK591 is a protein arginine methyltransferase 5 inhibitor that affects epigenetic

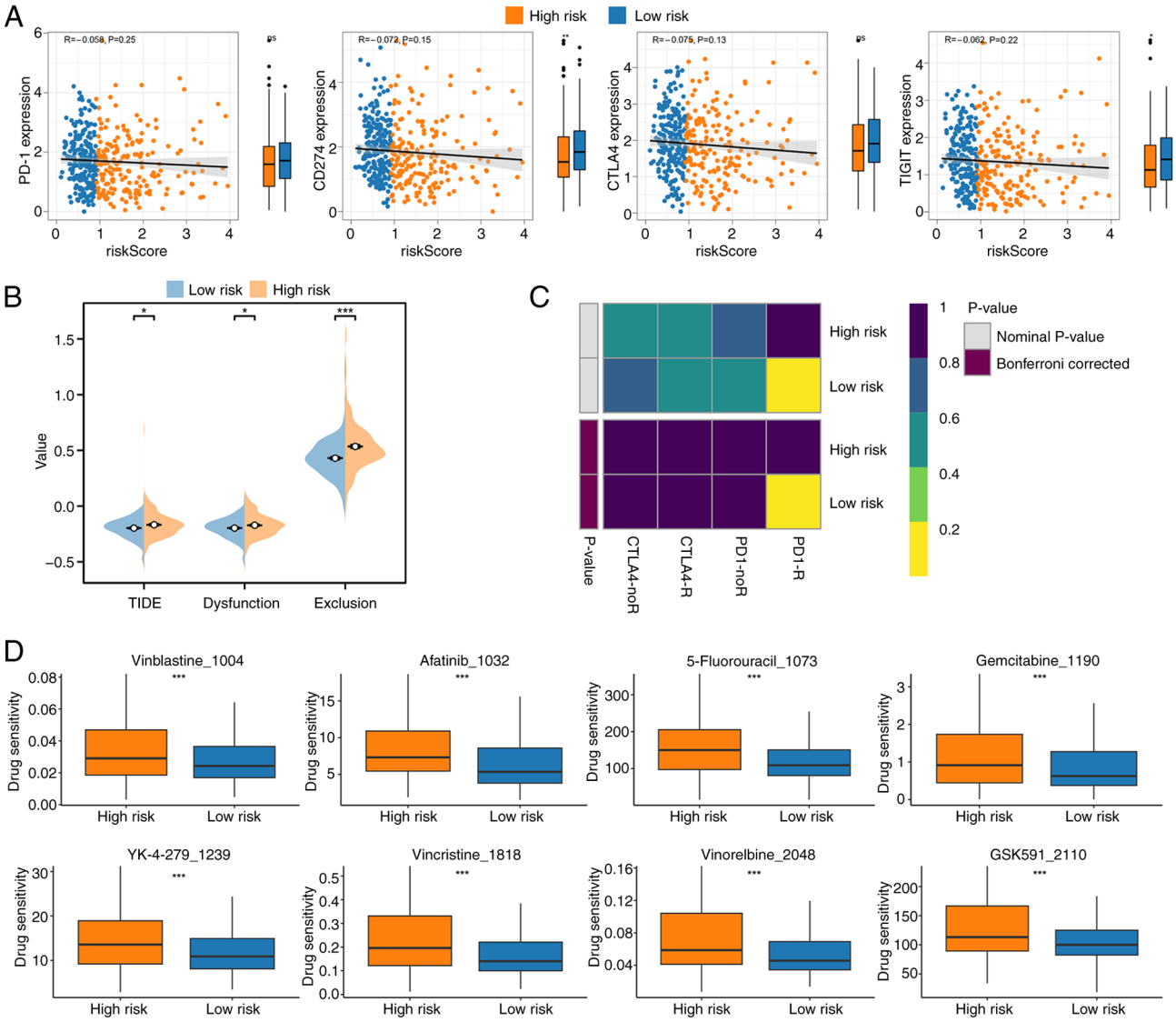

Figure 6. Treatment prediction analysis based on risk score. (A) Correlation analysis of risk score with the expression of immune checkpoint genes [PD-1, CD274 (PD-L1), CTLA4, TIGIT] and differential expression analysis, showing significantly higher expression in the low-risk group. (B) TIDE analysis demonstrating lower TIDE scores in the low-risk group, suggesting a greater likelihood of response to immune checkpoint inhibitors. (C) SubMap analysis further indicating enhanced sensitivity to immunotherapy in the low-risk group. (D) Drug sensitivity analysis from the GDSC database, highlighting the top eight drugs with the most significant differences in sensitivity between high- and low-risk groups. *P<0.05; ***P<0.001. PD-1, programmed cell death protein 1; PD-L1, programmed death-ligand 1; CTLA4, cytotoxic T-lymphocyte associated protein 4; TIGIT, T cell immunoreceptor with Ig and ITIM domains; TIDE, Tumor Immune Dysfunction and Exclusion.

regulation and has potential applications in several types of cancer (38). These findings provide a strong foundation for leveraging the risk signature to guide personalized treatment strategies, including both immunotherapy and targeted drug therapies.

Effects of KRT8P12 on CRC cells. KRT8P12 is a gene associated with palmitoylation. To verify the regulatory effect of KRT8P12 on CRC cells, the expression of the KRT8P12 gene was assessed in CRC cell lines HCT116 and HT29 using qPCR. Higher expression was demonstrated in HCT116 cells (Fig. 7A). The expression of KRT8P12 was subsequently knocked down in the HCT116 cell line using shRNA lentiviruses (sh-KRT8P12-3) and overexpression was performed in the HT29 cell line (OE-KRT8P12) (Fig. 7B). Since the target sequence of sh-KRT8P12-2 was absolutely matched with KRT8, it might also knock down KRT8, so it was not chosen for subsequent experiments. Subsequently, the proliferation of the constructed cell lines was assessed and it was demonstrated that sh-KRT8P12 decreased the proliferation of CRC cells, whereas overexpression of KRT8P12 promoted the proliferation of CRC cells. By contrast, 2-BP inhibited the proliferation induced by KRT8P12 overexpression (Figs. 7C and 8A). The effect of KRT8P12 on cell migration was evaluated using Transwell chambers, and it was demonstrated that silencing of KRT8P12 reduced the migration of CRC cells, whereas KRT8P12 overexpression significantly promoted tumor cell migration. Treatment with 2-BP inhibited the migration induced by KRT8P12 overexpression (Fig. 8B). The effect of KRT8P12 on CRC cell apoptosis was assessed using Annexin-V/PI staining, and it was demonstrated that sh-KRT8P12 enhanced apoptosis in CRC cells. Furthermore, 2-BP reversed the effect of KRT8P12 overexpression on inhibiting apoptosis (Fig. 9). In

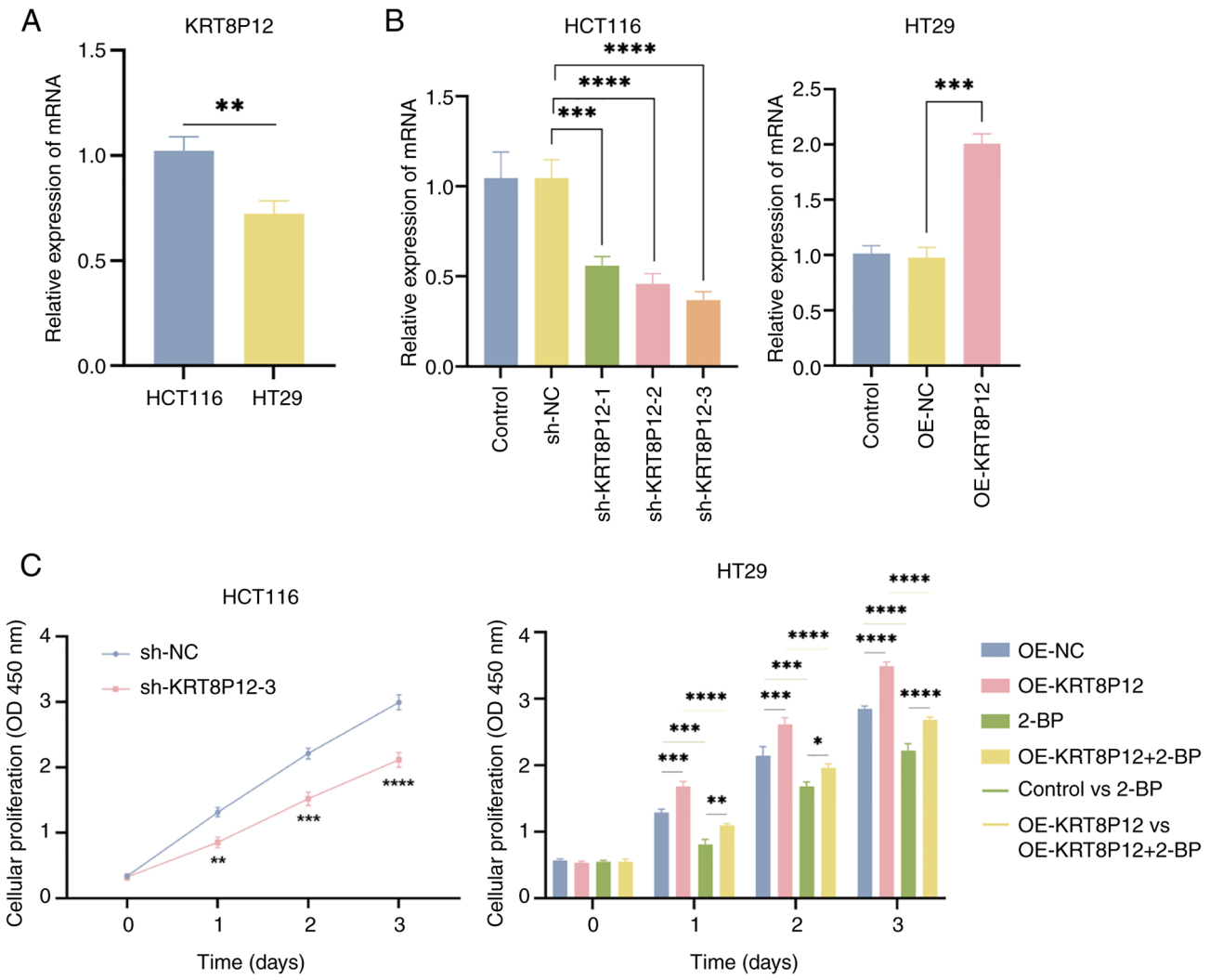

Figure 7. Regulation of colorectal cancer cell proliferation by KRT8P12. (A) Quantitative PCR analysis of KRT8P12 gene expression levels. (B) Validation of KRT8P12 knockdown and overexpression. (C) Cell Counting Kit-8 assay was performed to assess cell proliferation. *P<0.05; **P<0.01; ***P<0.001; ****P<0.0001 vs. shNC or as indicated. Each experiment was performed independently at least three times. KRT8P12, keratin 8 pseudogene 12; sh, short hairpin; OE, overexpression; NC, negative control; 2-BP, 2-bromopalmitate.

conclusion, the palmitoylation-associated gene KRT8P12 may promote tumor cell proliferation and migration, while inhibiting tumor cell apoptosis.

Discussion

CRC remains a leading cause of cancer-associated mortality, with a poor prognosis in advanced stages (39). Despite notable advances in treatment, patient outcomes are often hindered by late-stage diagnosis and a lack of effective prognostic biomarkers. Palmitoylation, a reversible post-translational modification, serves a critical role in regulating protein function, membrane localization and cellular signaling (40). Previous studies have suggested that alterations in palmitoylation may contribute to tumorigenesis and metastasis in CRC, underscoring its potential as a therapeutic target and prognostic marker (41,42).

In the present study, a palmitoylation-related prognostic signature was developed for CRC, which was validated using both TCGA and GSE17538 datasets. The findings demonstrated that this signature, comprising six key genes (KRT8P12, ZDHHC3, PCOLCE2, MPP2, LARS2 and MMAA), was significantly associated with OS in patients with CRC. Patients stratified into high- and low-risk groups based on this signature exhibited distinct clinical outcomes, with high-risk patients showing significantly worse survival. Notably, the signature was associated with immune cell infiltration, immune checkpoint gene expression and TMB, suggesting it has potential in predicting therapeutic responses, particularly to immunotherapy.

PD-1/PD-L1 has emerged as a prominent strategy in immunotherapy, serving a vital role in the treatment of various tumors (43). Concurrently, palmitoylation, as a post-translational modification, is increasingly being explored in the context of tumor immunotherapy (44). The application of 2-BP to inhibit the palmitoylation of PD-L1 or silencing of ZDHHC3 has demonstrated the ability to activate antitumor immunity both *in vitro* and in mice bearing MC38 tumor cells (45). Furthermore, Benzosceptrin C can prevent the palmitoylation of PD-L1 by inhibiting ZDHHC3 enzyme activity. This leads to the translocation of PD-L1 from the plasma membrane to the cytoplasm, preventing its recycling

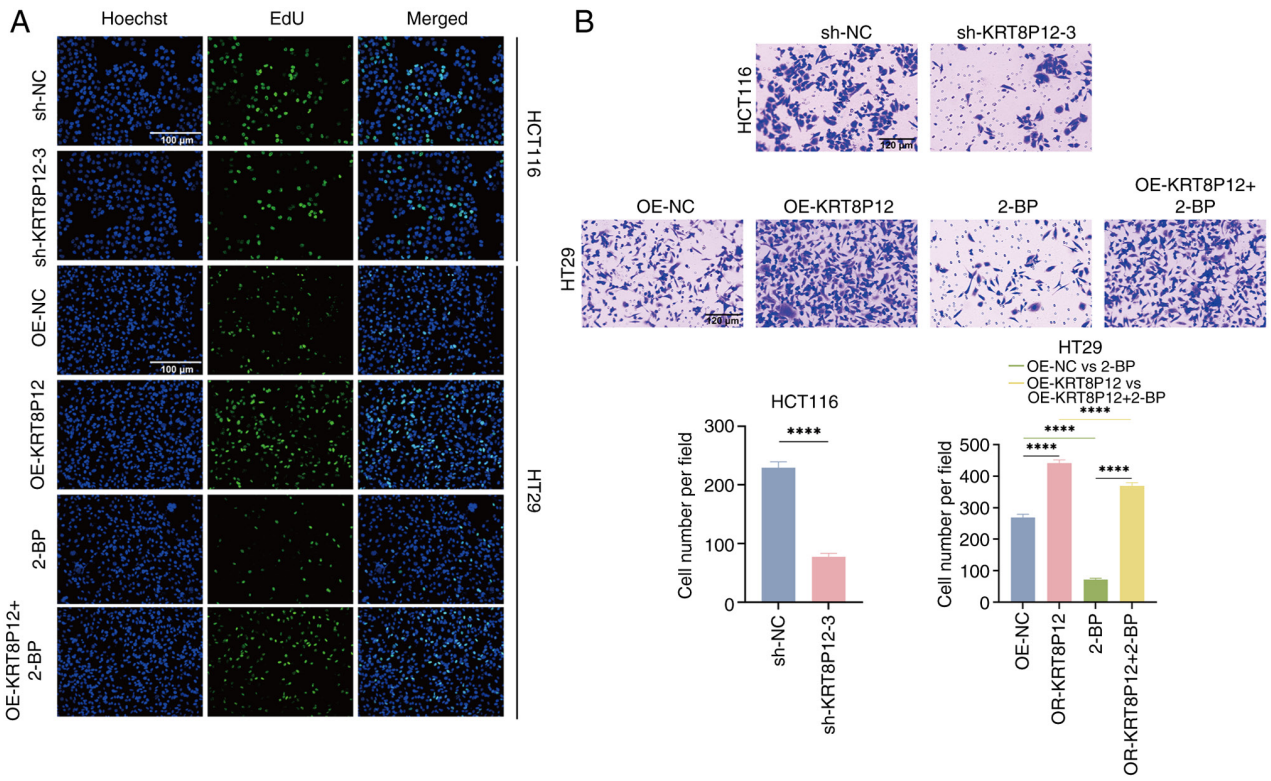

Figure 8. Regulation of colorectal cancer cell proliferation and migration by KRT8P12. (A) EdU assay was performed to evaluate cell proliferation. (B) Transwell assay was conducted to measure cell migration. ****P<0.0001. Each experiment was performed independently at least three times. KRT8P12, keratin 8 pseudogene 12; OE, overexpression; sh, short hairpin; EdU, 5-ethynyl-2'-deoxyuridine; NC, negative control; 2-BP, 2-bromopalmitate.

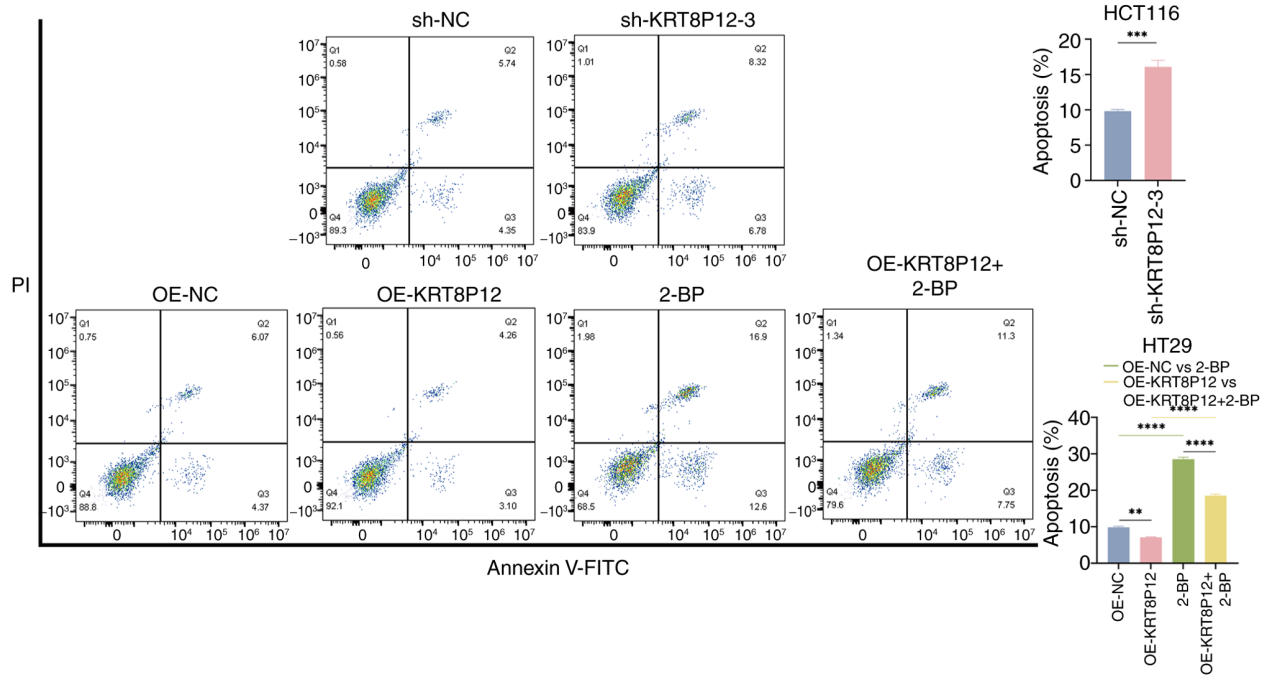

Figure 9. Regulation of colorectal cancer cell apoptosis by KRT8P12. Annexin-V/PI staining was performed to detect cell apoptosis. **P<0.01; ***P<0.001; ****P<0.0001. Each experiment was performed independently at least three times. KRT8P12, keratin 8 pseudogene 12; OE, overexpression; sh, short hairpin; NC, negative control; 2-BP, 2-bromopalmitate.

back to the membrane via endosomes, thereby triggering lysosomal degradation of PD-L1. Additionally, the combination of Benzosceptrin C with anti-CTLA4 antibodies effectively enhances antitumor T cell immunity (46). However, the therapeutic mechanisms of palmitoylation in CRC warrant further investigation.

The six key genes included in the palmitoylation-related prognostic signature, KRT8P12, ZDHHC3, PCOLCE2, MPP2, LARS2 and MMAA, are integral to the molecular mechanisms underlying the development and progression of CRC. To the best of our knowledge, KRT8P12, a key molecule in the present study, has not yet been reported to serve a role in CRC. However, members of the same family KRT8 and KRT19, which are associated with keratin production, may serve a role in tumor biology, particularly in CRC, where their expression levels can influence tumor behavior and patient prognosis (47). A previous study reported that ZDHHC3 expression is markedly downregulated in CRC, and higher expression levels of ZDHHC3 are associated with improved patient prognosis (48). Moreover, immunohistochemical analysis of CRC clinical samples has revealed that PCOLCE2 expression is markedly higher in tumor tissue compared with that in normal tissue. Knockdown experiments further demonstrated that silencing PCOLCE2 expression can notably reduce the proliferative capacity and epithelial-to-mesenchymal transition process in CRC cells (49). A previous study revealed that MPP2 is associated with the prognosis of several types of cancer, particularly CRC, and its expression level may notably influence patient survival rates (50). The LATS2 gene is regarded as a potential tumor suppressor, with its dysregulation implicated in tumorigenesis and cancer progression. A previous study reported a strong association between LATS2 expression levels, EGFR mutations and patient survival (51). In CRC, altered LATS2 expression may influence the regulation of cell proliferation and apoptosis, thereby impacting tumor progression. Together, these findings highlight the crucial roles of KRT8P12, ZDHHC3, PCOLCE2, MPP2, LATS2 and MMAA in the pathophysiology of CRC, suggesting that these genes may serve as potential biomarkers for prognosis and therapeutic targets in CRC management.

Functional enrichment analysis revealed that the palmitoylation-related risk signature was associated with critical pathways involved in tumorigenesis, including protein localization, signal transduction and intermediate filament dynamics. Notably, the high-risk group exhibited stronger enrichment in pathways associated with cell structure and metastasis such as 'cAMP signaling pathway' and 'intermediate filament', suggesting a potential role in CRC progression. These findings underscore the molecular mechanisms underlying the signature, highlighting its potential as a therapeutic target in CRC.

Immune cell infiltration analysis revealed significant differences between the high- and low-risk groups, with the low-risk group exhibiting higher levels of immune cell abundance, suggesting a more active antitumor immune response. Moreover, the low-risk group demonstrated increased expression of immune checkpoint genes, including PD-1, PD-L1 and CTLA4, indicating a greater potential for response to immune checkpoint inhibitors. TIDE analysis further supported these findings, revealing that the low-risk group had lower immune evasion scores, suggesting a higher likelihood of benefiting from PD-1/PD-L1 blockade. Additionally, SubMap analysis, which predicts responses to immunotherapy based on gene expression profiles, indicated that patients in the low-risk group might experience improved therapeutic outcomes with immune checkpoint inhibitors. Collectively, these results indicated the prognostic value of the palmitoylation-related signature, not only in predicting survival but also in guiding personalized immunotherapy strategies for patients with CRC, particularly those likely to benefit from immune checkpoint blockade.

In the present study, KRT8P12 was found to significantly promote the proliferation and migration of HCT116 and HT29 CRC cells, while inhibiting apoptosis. This result is consistent with the role of keratins in other types of cancer, where they enhance tumor invasiveness by promoting cell proliferation and migration. For example, co-expression of K20 and K7 was said to be indicative of advanced CRC. In CRC, increased expression of K7 and K20 is associated with epithelial to mesenchymal transition, which usually indicates higher tumor invasiveness and reduced patient survival (52). Additionally, the use of 2-BP to inhibit palmitoylation effectively blocked these effects, further confirming the crucial role of KRT8P12 and palmitoylation in CRC cells. Notably, the expression levels of KRT8P12 varied across different cell lines, which may influence its specific role in different tumor environments. As evidenced in the present study, the expression levels of KRT8P12 were shown to vary in HCT116 and HT29 cell lines. In addition, it was demonstrated that KRT8P12 serves an important role in tumor progression by promoting the proliferation and migration of CRC cells and inhibiting apoptosis. This finding not only provides new insights into the role of keratins in CRC but also offers potential targets for future therapeutic strategies. Future research could further explore the specific molecular mechanisms of KRT8P12 and its role in different tumor microenvironments, to develop more effective treatments.

Despite the promising findings of the palmitoylation-related prognostic signature, there are several limitations to the present study. Firstly, the present research is mainly based on the retrieval of public databases, which contain relatively small sample sizes and are not updated in a timely manner. The main research object was palmitoylation, and the specific molecular mechanism of its regulation of CRC progression still requires extensive research. Therefore, the interpretation of the results needs further validation and supplementation. Meanwhile, the signature was primarily validated using public datasets (TCGA and GSE17538), which may have inherent biases and lack clinical validation in independent, real-world patient cohorts. Secondly, while the immune cell infiltration and immunotherapy prediction analyses provide valuable insights, the precise mechanisms underlying the relationship between palmitoylation and immune responses in CRC remain unclear and require further experimental investigation. Additionally, the present research suggested that KRT8P12 may modulate immune responses and promote the progression of CRC through palmitoylation pathways. A comprehensive review of the literature on KRT8P12 was performed and found that it represents a novel therapeutic target. However, the molecular mechanisms of KRT8P12 in regulating CRC remain underexplored and warrant further investigation. The present study also did not assess the potential interactions between the six key genes and other molecular pathways that could contribute to CRC progression, which warrants further exploration. Finally, although the signature demonstrated potential for guiding immunotherapy strategies, the lack of prospective clinical trials to validate its predictive power limits its clinical applicability. Future studies should aim to validate

the prognostic signature in larger, more diverse patient populations and explore the mechanistic roles of palmitoylation in CRC.

Acknowledgements

Not applicable.

Funding

No funding was received.

Availability of data and materials

The data generated in the present study may be requested from the corresponding author.

Authors' contributions

Study conception and design was performed by XW, JL and QW. XW, JL and ZW conducted the literature research, and performed the experimental studies, data acquisition, data analysis and statistical analysis. The manuscript was prepared by XW and JL. Manuscript review was performed by XW, JL, ZW and QW. XW, JL and QW confirm the authenticity of all the raw data. All authors read and approved the final version of the manuscript.

Ethics approval and consent to participate

Not applicable.

Patient consent for publication

Not applicable.

Competing interests

The authors declare that they have no competing interests.

References

1. Siegel RL, Giaquinto AN and Jemal A: Cancer statistics, 2024. CA Cancer J Clin 74: 12-49, 2024.
2. Benson AB III, Venook AP, Cederquist L, Chan E, Chen YJ, Cooper HS, Deming D, Engstrom PF, Enzinger PC, Fichera A, *et al*: Colon cancer, version 1.2017, NCCN clinical practice guidelines in oncology. J Natl Compr Canc Netw 15: 370-398, 2017.
3. Saltz L: Systemic therapy for metastatic colorectal cancer. J Natl Compr Canc Netw 11 (Suppl 5): S649-S652, 2013.
4. Zhang D, Zhao K, Han T, Zhang X, Xu X, Liu Z, Ren X, Zhang X, Lu Z and Qin C: Bisphenol A promote the cell proliferation and invasion ability of prostate cancer cells via regulating the androgen receptor. Ecotoxicol Environ Saf 269: 115818, 2024.
5. Marks KM, West NP, Morris E and Quirke P: Clinicopathological, genomic and immunological factors in colorectal cancer prognosis. Br J Surg 105: e99-e109, 2018.
6. Anaya YA, Bracho RP, Chauhan SC, Tripathi MK and Bandyopadhyay D: Small Molecule B-RAF inhibitors as anti-cancer therapeutics: Advances in discovery, development, and mechanistic insights. Int J Mol Sci 26: 2676, 2025.
7. Linder ME and Deschenes RJ: Palmitoylation: Policing protein stability and traffic. Nat Rev Mol Cell Biol 8: 74-84, 2007.
8. Salaun C, Greaves J and Chamberlain LH: The intracellular dynamic of protein palmitoylation. J Cell Biol 191: 1229-1238, 2010.
9. Tape CJ, Ling S, Dimitriadi M, McMahon KM, Worboys JD, Leong HS, Norrie IC, Miller CJ, Poulogiannis G, Lauffenburger DA and Jørgensen C: Oncogenic KRAS regulates tumor cell signaling via stromal reciprocation. Cell 165: 1818, 2016.
10. Bivona TG: Dampening oncogenic RAS signaling. Science 363: 1280-1281, 2019.
11. Galluzzo P, Caiazza F, Moreno S and Marino M: Role of ERbeta palmitoylation in the inhibition of human colon cancer cell proliferation. Endocr Relat Cancer 14: 153-167, 2007.
12. Caiazza F, Galluzzo P, Lorenzetti S and Marino M: 17Beta-estradiol induces ERbeta up-regulation via p38/MAPK activation in colon cancer cells. Biochem Biophys Res Commun 359: 102-107, 2007.
13. Schwab RHM, Amin N, Flanagan DJ, Johanson TM, Phesse TJ and Vincan E: Wnt is necessary for mesenchymal to epithelial transition in colorectal cancer cells. Dev Dyn 247: 521-530, 2018.
14. Klaus C, Schneider U, Hedberg C, Schütz AK, Bernhagen J, Waldmann H, Gassler N and Kaemmerer E: Modulating effects of acyl-CoA synthetase 5-derived mitochondrial Wnt2B palmitoylation on intestinal Wnt activity. World J Gastroenterol 20: 14855-14864, 2014.
15. Dubois F, Leroy C, Simon V, Benistant C and Roche S: YES oncogenic activity is specified by its SH4 domain and regulates RAS/MAPK signaling in colon carcinoma cells. Am J Cancer Res 5: 1972-1987, 2015.
16. Draper JM and Smith CD: DHHC20: A human palmitoyl acyltransferase that causes cellular transformation. Mol Membr Biol 27: 123-136, 2010.
17. Rossin A, Durivault J, Chakhtoura-Feghali T, Lounnas N, Gagnoux-Palacios L and Hueber AO: Fas palmitoylation by the palmitoyl acyltransferase DHHC7 regulates Fas stability. Cell Death Differ 22: 643-653, 2015.
18. Kristensen VN, Lingjærde OC, Russnes HG, Vollan HK, Frigessi A and Børresen-Dale AL: Principles and methods of integrative genomic analyses in cancer. Nat Rev Cancer 14: 299-313, 2014.
19. Rich JT, Neely JG, Paniello RC, Voelker CC, Nussenbaum B and Wang EW: A practical guide to understanding Kaplan-Meier curves. Otolaryngol Head Neck Surg 143: 331-336, 2010.
20. Yu G, Wang LG, Han Y and He QY: clusterProfiler: An R package for comparing biological themes among gene clusters. OMICS 16: 284-387, 2012.
21. Mayakonda A, Lin DC, Assenov Y, Plass C and Koeffler HP: Maftools: Efficient and comprehensive analysis of somatic variants in cancer. Genome Res 28: 1747-1756, 2018.
22. Chalmers ZR, Connelly CF, Fabrizio D, Gay L, Ali SM, Ennis R, Schrock A, Campbell B, Shlien A, Chmielecki J, *et al*: Analysis of 100,000 human cancer genomes reveals the landscape of tumor mutational burden. Genome Med 9: 34, 2017.
23. Mermel CH, Schumacher SE, Hill B, Meyerson ML, Beroukhim R and Getz G: GISTIC2.0 facilitates sensitive and confident localization of the targets of focal somatic copy-number alteration in human cancers. Genome Biol 12: R41, 2011.
24. Powers RK, Goodspeed A, Pielke-Lombardo H, Tan AC and Costello JC: GSEA-InContext: Identifying novel and common patterns in expression experiments. Bioinformatics 34: i555-i564, 2018.
25. Newman AM, Steen CB, Liu CL, Gentles AJ, Chaudhuri AA, Scherer F, Khodadoust MS, Esfahani MS, Luca BA, Steiner D, *et al*: Determining cell type abundance and expression from bulk tissues with digital cytometry. Nat Biotechnol 37: 773-782, 2019.
26. Jiang P, Gu S, Pan D, Fu J, Sahu A, Hu X, Li Z, Traugh N, Bu X, Li B, *et al*: Signatures of T cell dysfunction and exclusion predict cancer immunotherapy response. Nat Med 24: 1550-1558, 2018.
27. Jiang P, Gu S, Pan D, Fu J, Sahu A, Hu X, Li Z, Traugh N, Bu X, Li B, *et al*: Signatures of T cell dysfunction and exclusion predict cancer immunotherapy response. Nat Med 24: 1550-1558, 2018.
28. Hoshida Y, Brunet JP, Tamayo P, Golub TR and Mesirov JP: Subclass mapping: Identifying common subtypes in independent disease data sets. PLoS One 2: e1195, 2007.
29. Geeleher P, Cox N and Huang RS: pRRophetic: An R package for prediction of clinical chemotherapeutic response from tumor gene expression levels. PLoS One 9: e107468, 2014.
30. Livak KJ and Schmittgen TD: Analysis of relative gene expression data using real-time quantitative PCR and the 2(-Delta Delta C(T)) method. Methods 25: 402-408, 2001.
31. Sebastian J and Rathinasamy K: Microtubules and cell division: Potential pharmacological targets in cancer therapy. Curr Drug Targets 24: 889-918, 2023.

32. Chen L, Chen WD, Xu YX, Ren YY, Zheng C, Lin YY and Zhou JL: Strategies for enhancing non-small cell lung cancer treatment: Integrating Chinese herbal medicines with epidermal growth factor receptor-tyrosine kinase inhibitors therapy. Eur J Pharmacol 980: 176871, 2024.
33. Lin JC, Oludare A and Jung H: Connecting dots between nucleotide biosynthesis and DNA lesion repair/bypass in cancer. Biosci Rep 44: BSR20231382, 2024.
34. Jordheim LP: Clinical use of biomarkers in the field of cytotoxic nucleoside analogues. Nucleosides Nucleotides Nucleic Acids 43: 822-830, 2024.
35. Conn E, Hour S, Allegakoen D, Graham G, Petro J, Kouassi-Brou M, Hong SH, Selvanathan S, Çelik H, Toretsky J and Üren A: Development of an Ewing sarcoma cell line with resistance to EWS-FLI1 inhibitor YK-4-279. Mol Med Rep 21: 1667-1675, 2020.
36. Banyal A, Tiwari S, Sharma A, Chanana I, Patel SKS, Kulshrestha S and Kumar P: Vinca alkaloids as a potential cancer therapeutics: Recent update and future challenges. 3 Biotech 13: 211, 2023.
37. Sun K, Sun Z, Zhao F, Shan G and Meng Q: Recent advances in research of colchicine binding site inhibitors and their interaction modes with tubulin. Future Med Chem 13: 839-858, 2021.
38. Sun J, Yuan H, Sun L, Zhao L, Wang Y, Hou C, Zhang H, Lv P, Yang G, Zhang N, *et al*: Tumor-intrinsic PRMT5 upregulates FGL1 via methylating TCF12 to inhibit CD8+ T-cell-mediated antitumor immunity in liver cancer. Acta Pharm Sin B 15: 188-204, 2025.
39. Eng C, Yoshino T, Ruíz-García E, Mostafa N, Cann CG, O'Brian B, Benny A, Perez RO and Cremolini C: Colorectal cancer. Lancet 404: 294-310, 2024.
40. Liu Z, Xiao M, Mo Y, Wang H, Han Y, Zhao X, Yang X, Liu Z and Xu B: Emerging roles of protein palmitoylation and its modifying enzymes in cancer cell signal transduction and cancer therapy. Int J Biol Sci 18: 3447-3457, 2022.
41. Zhu J, Cao X, Chen Z, Lai B, Xi L, Zhang J, Zhu S, Qi S, Liang Y, Cao F, *et al*: Inhibiting S-palmitoylation arrests metastasis by relocating Rap2b from plasma membrane in colorectal cancer. Cell Death Dis 15: 675, 2024.
42. Kong Y, Liu Y, Li X, Rao M, Li D, Ruan X, Li S, Jiang Z and Zhang Q: Palmitoylation landscapes across human cancers reveal a role of palmitoylation in tumorigenesis. J Transl Med 21: 826, 2023.
43. Tsai MY, Lu CK, Shu LH, Liu HT, Wu YH, Lin YS, Yang YH, Shih WT, Lee IY, Wu YH and Wu CY: *Antrodia cinnamomea* formula suppresses prostate cancer progression via immune modulation and PD-1/PD-L1 pathway inhibition. Int J Mol Sci 26: 2684, 2025.
44. Lee TA, Tsai EY, Liu SH, Hsu Hung SD, Chang SJ, Chao CH, Lai YJ, Yamaguchi H and Li CW: Post-translational modification of PD-1: Potential targets for cancer immunotherapy. Cancer Res 84: 800-807, 2024.
45. Yao H, Lan J, Li C, Shi H, Brosseau JP, Wang H, Lu H, Fang C, Zhang Y, Liang L, *et al*: Inhibiting PD-L1 palmitoylation enhances T-cell immune responses against tumours. Nat Biomed Eng 3: 306-317, 2019.
46. Wang Q, Wang J, Yu D, Zhang Q, Hu H, Xu M, Zhang H, Tian S, Zheng G, Lu D, *et al*: Benzosceptrin C induces lysosomal degradation of PD-L1 and promotes antitumor immunity by targeting DHHC3. Cell Rep Med 5: 101357, 2024.
47. Wang W, He J, Lu H, Kong Q and Lin S: KRT8 and KRT19, associated with EMT, are hypomethylated and overexpressed in lung adenocarcinoma and link to unfavorable prognosis. Biosci Rep 40: BSR20193468, 2020.
48. Zhang, X, Hou J, Zhou G, Wang H and Wu Z: zDHHC3-mediated S-palmitoylation of SLC9A2 regulates apoptosis in kidney clear cell carcinoma. J Cancer Res Clin Oncol 150: 194, 2024.
49. Yin Y, Yang X, Cheng Z, Wang H, Lei J, Wang D, Wang P, Li B, Mi J and Yuan Q: Identification of extracellular matrix-related biomarkers in colon adenocarcinoma by bioinformatics and experimental validation. Front Immunol 15: 1371584, 2024.
50. Tang L, Yu S, Zhang Q, Cai Y, Li W, Yao S and Cheng H: Identification of hub genes related to CD4(+) memory T cell infiltration with gene co-expression network predicts prognosis and immunotherapy effect in colon adenocarcinoma. Front Genet 13: 915282, 2022.
51. Luo SY, Sit KY, Sihoe AD, Suen WS, Au WK, Tang X, Ma ES, Chan WK, Wistuba II, Minna JD, *et al*: Aberrant large tumor suppressor 2 (LATS2) gene expression correlates with EGFR mutation and survival in lung adenocarcinomas. Lung Cancer 85: 282-292, 2014.
52. Karantza V: Keratins in health and cancer: More than mere epithelial cell markers. Oncogene 30: 127-138, 2011.